Association Aéronautique et Astronautique de France

59th 3AF International Conference on Applied Aerodynamics
24 – 26 March 2025, Strasbourg - France

AERO2025-21

Unsteady flow interactions and ground plane proximity in a coupled compact intake-fan in crosswind

L. Lobuono[(1)], D. MacManus[(1)], J. Hueso-Rebassa[(1)] and R. Christie[(1)]
[(1)] Cranfield University, Cranfield, Bedfordshire, MK43 0AL, United Kingdom
Corresponding Author's Email:luca.lobuono.030@cranfield.ac.uk

ABSTRACT

The assessment of the crosswind flow separation mechanisms and resulting distortion for compact intakes can be a key contributor for the design of viable large civil aeroengines. Under crosswind conditions, the intake aerodynamics are strongly influenced by both the fan and the ground plane. However, the impact of key design parameters, such as ground clearance, on the intake flow distortion is not fully understood. This study investigates the effects of a large variation in ground clearance on the intake-fan unsteady aerodynamics using an Unsteady Reynolds-Averaged Navier-Stokes fully coupled with a rotating fan stage. The work includes an assessment of the unsteady swirl distortion and the unsteady peak distortion events. The findings show that increased ground clearance can have adverse effects for the considered compact intake design. Gross separation can occur at lower crosswind velocities and arise at the intake lower section due to mass flow redistribution. When the ground clearance is increased, the gross separation on the windward side of the intake occurs at a greater crosswind velocity but exhibits greater levels of unsteady intake flow distortion. Overall, intake designs should be assessed at the expected ground clearance as the distortion and the onset of separation can vary substantially.

1. Introduction

The design of aero-engine intakes is a key aspect in reducing cruise fuel consumption by minimizing cruise drag and mass of the overall propulsion system. Compact intakes can offer benefits [1] but pose challenges under high incidence and crosswind conditions [2]. For these operating conditions boundary layer separations can arise on the intake surface due to shocks on the lip or local subsonic diffusion. Additionally, the impact of features such as the ground vortex (GV), upstream perturbations from the fan, and intake flow unsteadiness remain insufficiently understood.

In crosswind operations, the conditions under which the intake flow separates are influenced by the crosswind velocity (V_{cw}) and mass flow capture ratio MFCR= $m_f/(\rho_\infty A_{hi} V_{cw})$, where m_f, ρ_∞, A_{hi} are the intake mass flow, freestream density, and highlight area, respectively. Piovesan et al [3] investigated the intake aerodynamics for different combinations of these parameters using Particle Image Velocimetry (PIV) measurements within an aspirated turbofan intake. Two distinct types of separation were identified, one related to subsonic diffusion (low MFCR) and a shock-induced separation (high MFCR). These are critical considerations to understand the operational limits of an intake in crosswind conditions. The separated regions are characterised by total pressure losses and extensive flow distortion which have the potential to act as initiators of fan stall [4], [5], [6].

The ground vortex and trailing vortices also contribute to intake flow distortion by inducing pressure loss and swirl at the Aerodynamic Interface Plane (AIP) [7], [8], [9], [10]. Previous work [7] indicates that the ground clearance significantly impacts the formation and strength of ground vortices. The intake ground clearance, along with the approaching boundary layer thickness and freestream Mach number can notably affect the vortex strength [7]. As ground clearance decreases, the interaction between the intake stream tube and the ground intensifies, which can lead to an increase in the ground vortex strength and the associated level of distortion [7], [10].

For shorter and more compact intakes, the fan and intake aerodynamics are closely coupled. Research shows that the fan can positively influence intake performance under high incidence by redistributing mass flow and accelerating flow at the fan tip which can alleviate the local adverse pressure gradients [2].

Published by 3AF. This is the Author Accepted Manuscript issued with: Creative Commons Attribution License (CC:BY 4.0).
The final published version (version of record) is available online at DOI:10.60711/aero2025.20250401.8402130248130544.
Please refer to any applicable publisher terms of use.

However, unsteady fan effects, such as unsteady pressure waves, can propagate upstream and reduce the crosswind speed threshold for stable intake operation [11], [12]. Previous studies [13] of conventional and short intakes under crosswind conditions highlight that shorter intakes reduce the extent of the intake flow separation but may increase swirl variation in the separated region, particularly for counter-rotating configurations.

Previous studies have examined the influence of intake–ground plane interaction on the formation and strength of the ground vortex [7], [8], [9], [10], [14]. However, the work has not explored the effects on intake separation mechanisms and unsteady flow distortion. Much of the prior research primarily focused on aspirated intake configurations without considering the interaction with the fan. This current study builds upon previous research and methodologies that investigated unsteady intake-fan interactions under crosswind conditions [15]. While prior work analysed the intake flow separation, and spectral characteristics of distortion, the key contribution of this study lies in the identification of the intake separation mechanisms and the swirl distortion due to significant changes in ground clearance. The unsteady swirl distortion is assessed using a blade incidence tracking method that quantifies both the intensity and azimuthal extent of peak swirl distortion events. This method is applied for the first time to a full-scale compact intake, providing new insights into its aerodynamic behaviour.

2. Methodology

2.1. Intake design and computational grid

The in-house Tool for Intake Design (TIDE)[16], [17] method was used to design the intake geometry. A 3D non-axisymmetric intake was generated using a parametric approach based on iCST curves. The full-scale configuration consists of a compact intake with a length-to-fan-diameter ratio (L_{in}/D_{fan}) of 0.4 [15]. A significant variation in ground clearance was evaluated for H/D_{hi}=0.25 and H/D_{hi}=0.44, where H denotes the height of the bottom lip above the ground and D_{hi} is the highlight diameter (Figure 1). A fully structured 3D mesh consisting of 4×10^7 cells was used. This is based on the grid independence and validation studies carried out by Boscagli et al [11]. The wall boundary layer was resolved with a y^+=1. The computational domain is approximately a quarter-sphere with a radius about 30 times the fan diameter, based on [18]. Static pressure far-field boundary conditions are applied at the freestream, while the intake, fan cowl, spinner, and ground plane are modelled as no-slip walls (based on [11]).

2.2. Solver & coupled intake-fan CFD analysis

The simulations are conducted using a proprietary Navier Stokes code, which is an unstructured finite volume solver [19], [20]. The unsteady computations are performed with an explicit solver. The aerodynamic interaction between the intake and the fan is investigated with an unsteady fully coupled intake-fan CFD approach. The work followed the methodology outlined by Boscagli et al. [11], [12], [21]. This technique utilizes an unsteady Reynolds Averaged Navier-Stokes (URANS) approach with a fully rotating annulus fan, referred to as URANS-Time Resolved Fan (URANS-TRF). The computational capabilities for the turbomachinery were validated by Boscagli et al [11] using a single research fan stage in isolation.

In this work, the simulation setup includes an intake coupled with the research fan stage, featuring a single passage Outlet Guide Vane (OGV) and Engine Sector Stator (ESS) blades (Figure 1). A sliding plane boundary condition is implemented at the interface between the full annulus fan and intake, while a mixing-plane boundary condition is applied between the fan-OGV and fan-ESS regions. Constant mass flow rates are set at the OGV and ESS exits.

Building on previous computational analyses of intakes with body-force fan models [22], [23], [24], the Spalart-Allmaras (SA) turbulence model is applied. The URANS-TRF simulations are conducted with a computational frequency corresponding to 60 times the blade passing frequency (f_{bp}). Data sampling occurs every 12 timesteps, yielding a sampling frequency ratio of f_s/f_{bp}= 5. A frequency resolution of f_{res}/f_{bp} ~ 0.01 is achieved [15].

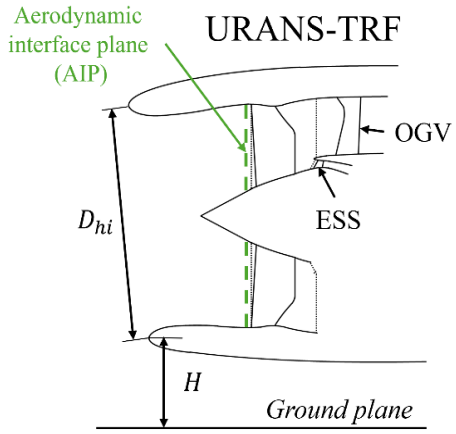


Figure 1 Schematic representation of intake-fan configuration.

2.3. Unsteady Post Processing

The distribution of aerodynamic quantities is assessed at the Aerodynamic Interface Plane (AIP, Figure 1), and on the unwrapped intake surface. The isentropic Mach number M_{isen} and axial wall shear stresses τ_{wx} are investigated on the intake surface.

The swirl and relative swirl angles are evaluated with Eq. (1) and (2), where V_θ and V_{ax} are the tangential and axial components of the absolute velocity, U denotes the peripherical velocity (Eq. (3)), and the term V_θ-U=W_θ is the relative tangential velocity. V_θ and W_θ are considered positive in the same direction of U; α, β and are considered positive in the clockwise direction, which is the same the fan rotational speed ω[rad/s].

$$\alpha = \tan^{-1}(V_\theta / V_{ax}) \quad (1)$$

$$\beta = \tan^{-1}((V_\theta - U)/V_{ax}) \quad (2)$$

$$U = \omega r \quad (3)$$

Considering this sign convention for β, the blade incidence angle i is calculated with Eq. (4), where β_m represents the blade metal angle. The variation of blade incidence angle Δi (Eq. (5)) is determined with reference to the nominal values of incidence i_{nom}. This is evaluated with a circumferential average of i for a steady single passage fan computation.

$$i = \beta_m - \beta \quad (4)$$

$$\Delta i = i - i_{nom} \quad (5)$$

The time variation of Δi is investigated and a discrete Fourier transform method implemented in a Fast Fourier Transform (FFT) algorithm [25] is used to analyse the spectrum of Δi.

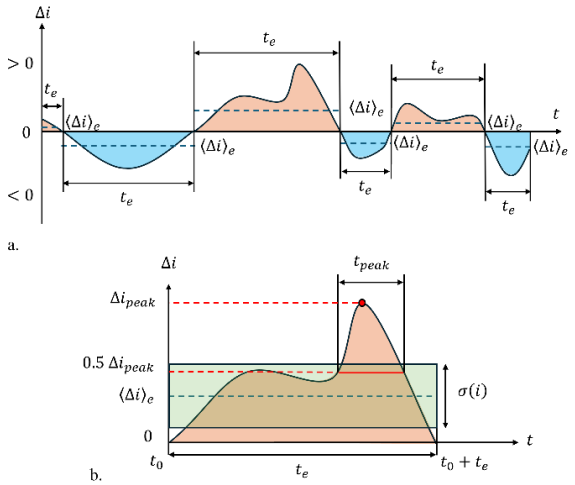


Figure 2 (a.) Time variation of Δi and blade distortion events; (b.) peak distortion event (based on [26]).

Δi is tracked for each blade and across the radial extent at the AIP. The method was outlined by Migliorini et al. [26] and defines a swirl distortion event as a strictly positive or strictly negative interval of Δi(t) (Figure 2 a). Each distortion event is characterised by a duration t_e and an average value $\langle\Delta i\rangle_e$. For each distortion event, the peak Δi_{peak} is identified. A distortion event is classified as a peak distortion event if the condition of Eq. (6) is satisfied (Figure 2 b). The standard deviation of blade incidence is denoted with σ(i).

$$\exists\, t_j \in [t_0, t_0 + t_e] \mid |\Delta i(t_j)| > |\langle\Delta i\rangle_e| + \frac{\sigma(i)}{2} \quad (6)$$

For each distortion peak event, the peak intensity is the maximum value Δi_{peak} and the duration of the peak event t_{peak} is defined by the time interval in which $|\Delta i| \geq 0.5|\Delta i_{peak}|$. The duration of the peak distortion event is expressed in terms of azimuthal exposure ϕ with Eq. (7).

$$\phi[°] = \omega t_{peak} \times \frac{180°}{\pi} \quad (7)$$

3. Results

3.1. Intake separation characteristics

For a relatively low ground clearance of H/D_{hi}=0.25 the flow is attached up to a crosswind velocity of V_{cw}=28 kts (Figure 3 a and Figure 4 a-b) since there is no large total pressure losses at the AIP. However, two specific regions of local separation are observed on the intake surface (Figure 4 a-b). A first type of unsteady separation (A1) arises from the shock boundary layer interaction at θ = 150º. Additional local pockets of unsteady separation (B) are associated with the impact of the unsteady fan static pressure pulses on the boundary layer of the intake diffuser [15]. These pressure pulses originate from the fan shocks and propagate upstream. Previous studies [11], [12] suggested that these local perturbations could propagate upstream to the front shock and exacerbate shock-boundary layer interactions. However, this is not observed in the current study which is for a different intake design. Instead, the pressure pulses primarily affect the flow in the diffuser, indicating that the fan unsteady effects may depend on the intake design. From V_{cw}= 22kts to 28kts the axial extent of the shock-driven separation increases until this starts to merge with the subsonic diffusion separations. For a crosswind velocity of V_{cw}=30kts, a second large windward separation arises from the lip (A2 in Figure 3 b and Figure 4 c). This extends towards the AIP and results in a notable loss in total pressure (Figure 3 b).

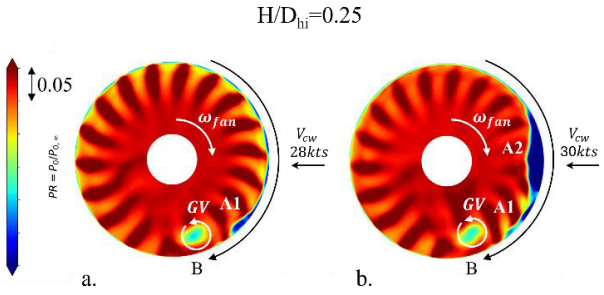


Figure 3 Snapshot of intake total pressure ratio for (a.) V_{cw}=28kts, H/D_{hi}=0.25, (b.) V_{cw}=30kts, H/D_{hi}=0.25.

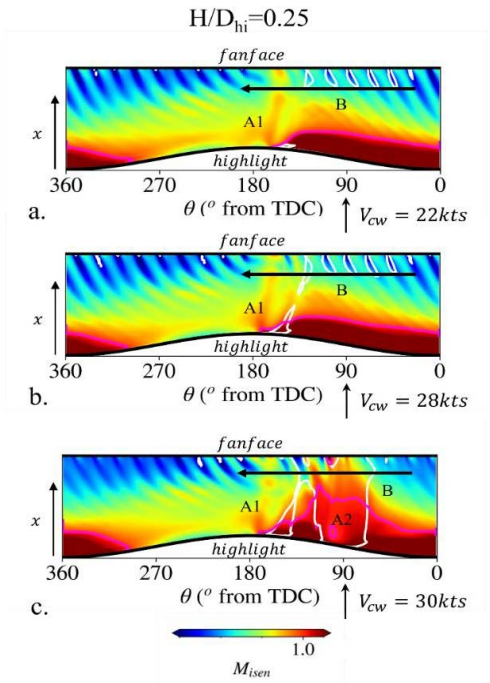


Figure 4 Snapshot of M_{isen} on the unwrapped intake surface with isoline of M_{isen}=1 (magenta), and axial wall shear stresses τ_{wx}=0 (white) for H/D_{hi}=0.25 at (a.) V_{cw}=22kts, (b.)V_{cw}=28kts, (c.) V_{cw}=30kts.

Notable differences in the separation onset arise when the ground clearance is increased from 0.25 (Figure 3, Figure 4) to 0.44 (Figure 5, Figure 6). For H/D_{hi}=0.44, the gross lip separation develops on the bottom lip at V_{cw}≥24knts (A1 in Figure 5 a and Figure 6b-c). The different origin of the intake separation is associated with a change in mass flow distribution and an increase in the intake lip loading at the bottom dead centre region (at θ~180º). For example, for the high ground clearance (H/D_{hi}=0.44) and V_{cw}=22kts (Figure 6 a) the sonic line extends up to θ=200º and the peak of M_{isen} is highly supersonic at θ=180º. Conversely, the flow around the bottom lip is subsonic for H/D_{hi}=0.25 (Figure 4 a). However, as expected, the onset of gross separation on the windward side is improved for H/D_{hi}=0.44 and arises at a higher crosswind velocity of 36knts (A2 in Figure 5 d and Figure 6 d) compared to H/D_{hi}=0.25. With higher ground clearance, the windward side has a reduced lip loading as more flow is redirected toward the bottom region of the intake. However, once flow separation occurs on the windward separation at V_{cw}=36kts, this becomes dominant, while the separation in the lower region mostly reattaches.

The change in ground clearance also affects the total pressure loss associated with the ground vortex. Relative to the low ground clearance (H/D_{hi}=0.25) the total pressure loss is reduced for H/D_{hi}=0.44 (Figure 5) and also confirms the expected reduction in the strength of the ground vortex [7], [9], [10]. There is a small change in the position of the ground vortex which moves to the leeward side of the intake when the ground clearance is increased. This can be associated with the different mass flow distribution. As more flow is redirected towards the bottom of the intake, the ground vortex migrates to the leeward side.

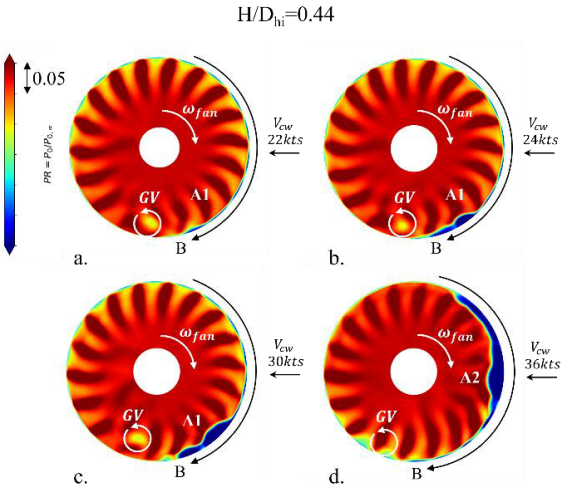


Figure 5 Snapshot of intake total pressure ratio for H/D_{hi}=0.44 at a. V_{cw}=22kts, b. V_{cw}=24kts, c. V_{cw} =30kts, d. V_{cw}=36kts.

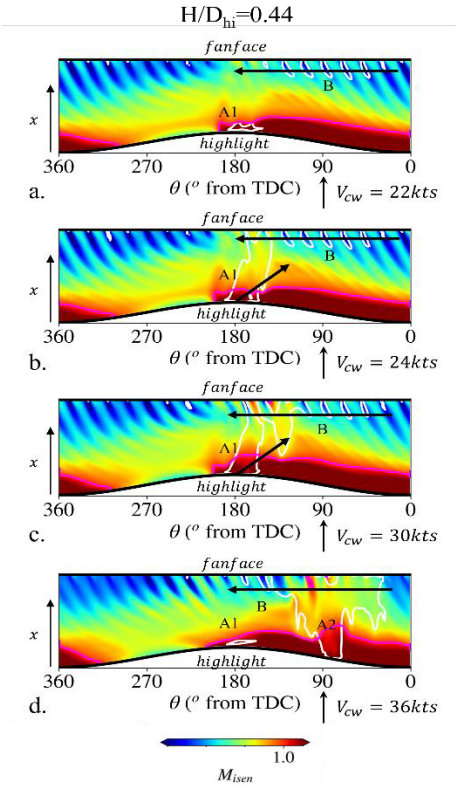


Figure 6 Snapshot of M_{isen} on the unwrapped intake surface with isoline of M_{isen}=1 (magenta), and axial wall shear stresses τ_{wx}=0 (white) for H/D_{hi}=0.44 at (a.) V_{cw}=22kts, (b.) V_{cw}=24kts, (c.) V_{cw}=30kts, (d.) V_{cw}=36kts.

Overall, these results demonstrate that the ground clearance can significantly affect the location of the gross flow separation within the intake. A higher ground clearance is not always beneficial as gross separation occurs at 6 kts lower V_{cw} compared to the H/D_{hi}=0.25 configuration for a specific intake design. However, the total pressure loss associated with the ground vortex and the onset of windward separation are improved because of the lower ground vortex strength and mass flow distribution. For H/D_{hi}=0.44, the main separation on the windward side occurs at 6kts higher V_{cw}, but this is more distorted than the equivalent critical condition for H/D_{hi}=0.25 (V_{cw}=30kts).

3.2. Swirl distortion characteristics

The variation of incidence (Δi) is mainly attributed to the change of two aerodynamic quantities, the swirl angle α and the axial velocity V_{ax}. Taking as a reference an ideal condition with uniform axial velocity $V_{ax}=V_{ax}^{id}$ (axial velocity in isentropic conditions) and α=0º, a positive Δi is generally due to either negative swirl angles (tangential velocity opposite to the fan rotation) or low or even negative values of V_{ax}. In contrast, positive swirl (tangential velocity in the same direction of the fan rotation) and higher axial velocity can reduce incidence (Δi<0).

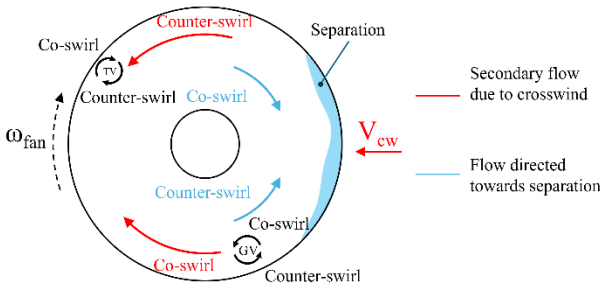
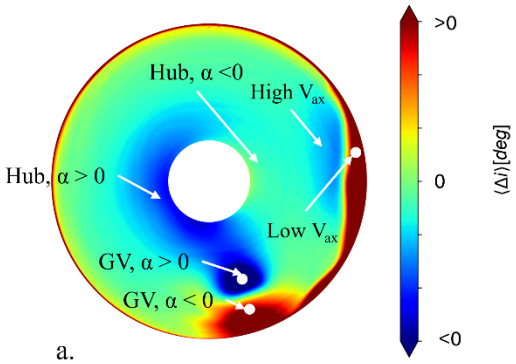


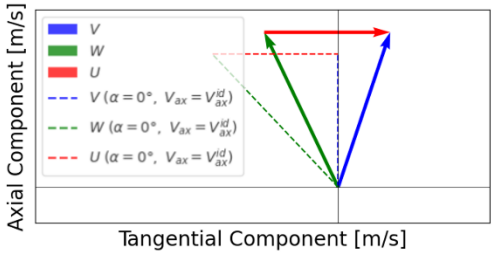
Figure 7 Secondary flows and vortices for an intake in crosswind for a counter-rotating configuration. Partially based on [13] .

According to Castillo Pardo et al. [13] three main types of secondary flows can be responsible for counter and co-swirl regions at the AIP. These effects are generated within coupled intakes-fan in crosswind because of the intake droop, flow turning of the captured stream tube, and the flow separation.

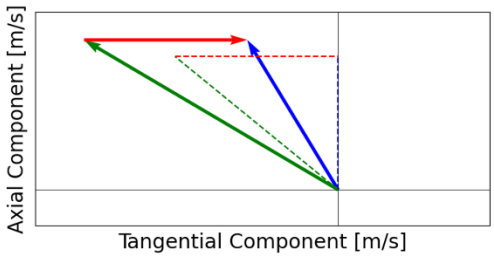
In the bottom-left part of the intake the co-swirl effects due to the crosswind direction (Figure 7) generates a region of positive swirl and Δi<0 (Figure 8 a). This is amplified at the hub. The counter-swirl effect on the top-right part of the intake (Figure 8 a) is not as evident as the co-swirl effect in the bottom-left region. The counter-swirl due to the crosswind direction is probably counter-balanced by the co-swirl that directs the flow towards the separation (Figure 7). The increase in axial velocity is much greater in the region adjacent to the separation and that results in Δi<0 on the windward side (Figure 8 a).



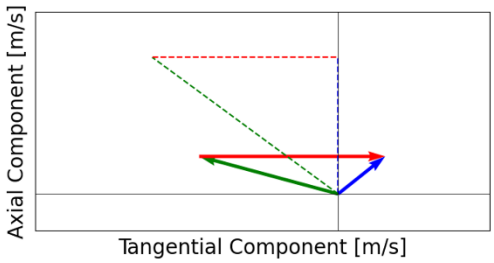
a.



b. GV, α > 0



c. GV, α < 0

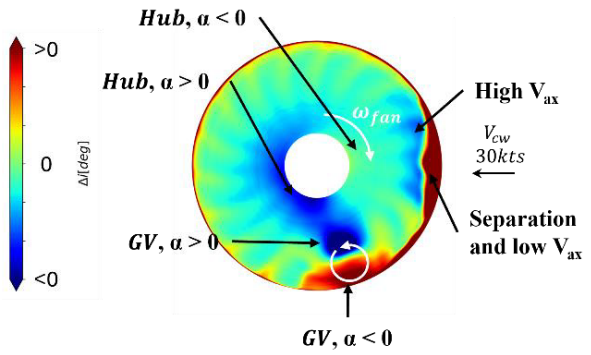


d. Low V_{ax}

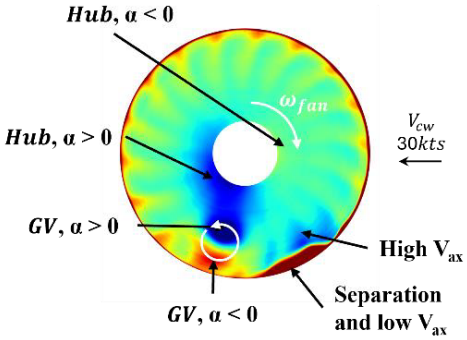
Figure 8 (a.) Time-averaged distribution of Δi for H/D_{hi}=0.25 and V_{cw}=30kts, time-averaged velocity triangles: (b) for the region of the GV with α>0, (c) for the region of the GV with α<0, (d) for the region at the tip with low V_{ax}.

The highest variation of blade incidence is observed in the separated flow regions and the ground vortex. For example, for the H/D_{hi}=0.25 configuration (Figure 8a) a

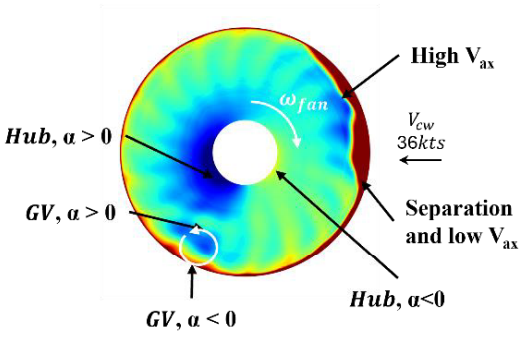
counter-rotating ground vortex generates a positive variation of incidence at the tip and negative variation in the inner side. The velocity triangles for the GV (Figure 8 b-c) are characterised by $V_{ax}>V_{ax}^{id}$, and Δi is dominated by $\alpha>0$ ($\Delta i<0$, Figure 8 b) and $\alpha<0$ ($\Delta i>0$, Figure 8 c) induced by the ground vortex. The flow in the separated region and in its immediate proximity is characterised by high magnitude of α (positive and negative); however, $\Delta i>>0$ is mainly associated with either small and positive V_{ax} (Figure 8d) or $V_{ax}<0$.



a. V_{cw}=30kts, H/D_{hi}=0.25



b. V_{cw}=30kts, H/D_{hi}=0.44



c. V_{cw}=36kts, H/D_{hi}=0.44

Figure 9 Snapshot of Δi for (a.) H/D_{hi}=0.25, V_{cw}=30kts, (b.) H/D_{hi}=0.44, V_{cw}=30kts, (c.) H/D_{hi}=0.44, V_{cw}=36kts.

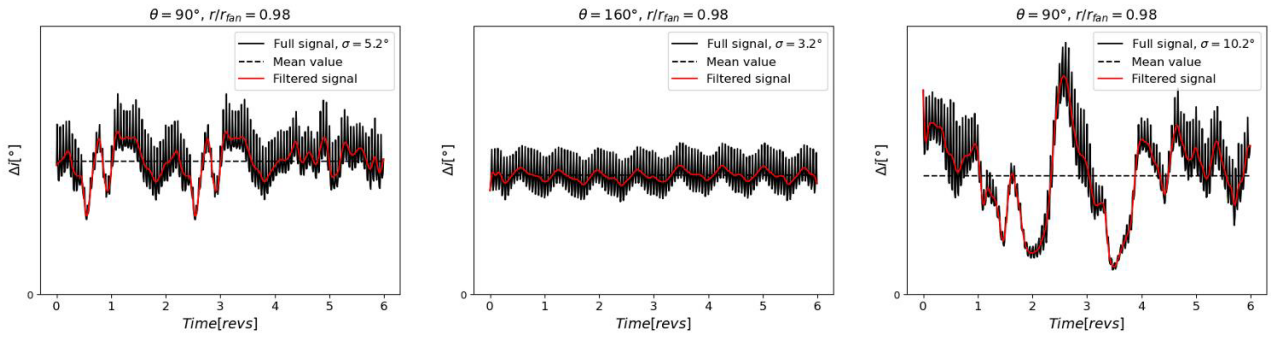
An additional trailing vortex can also originate on the leeward side. This vortex rotates in the direction opposite to the ground vortex (co-rotating for counter-rotating GV); it is usually considerably weaker than the ground vortex and does not result in significant changes in incidence on the leeward side (Figure 8 a).

The flow features within the intake are observed for the three configurations H/D_{hi}=0.25, V_{cw}=30kts (Figure 9 a), H/D_{hi}=0.44 and V_{cw}=30kts (Figure 9 b), H/D_{hi}=0.44 and V_{cw}=36kts (Figure 9 c). In all the three cases, the windward lip flow separation generates the maximum variation of incidence at the AIP. The windward separation of H/D_{hi}=0.25 and V_{cw}=30kts (Figure 9 a.) is associated with a larger extent of very high Δi regions compared to the bottom separation of H/D_{hi}=0.44 and V_{cw}=30kts (Figure 9 b). However, as the crosswind velocity is increased to V_{cw}=36kts the windward separation arises for the large ground clearance (Figure 9 c), and it extends for a larger azimuthal extent compared H/D_{hi}=0.25 and V_{cw}=30kts (Figure 9 a). The fan is likely to be exposed to regions with very high incidence at the tip and this can be detrimental for its operation [5]. Also, for H/D_{hi}=0.25 (Figure 9 a), the swirl associated with the ground vortex generates a greater variation of incidence. This is due to the increased strength of the GV. For H/D_{hi}=0.44 and V_{cw}=36kts (Figure 9 c), the ground vortex moves to the leeward side and towards the intake surface. That limits the radial extent of the negative and positive swirl regions associated with the GV, but the azimuthal extent of the distorted region is increased.

3.3. Unsteady swirl distortion

The unsteady features of swirl distortion can potentially have notable impact on the fan operation, as the time and spatial fluctuations of incidence can trigger fan stall [4], [5], [6]. In this section the temporal variation of incidence is evaluated for the dominant shock driven separation. For H/D_{hi}=0.25 and V_{cw}=30kts, the time variation of Δi is characterised by notable high incidence in the separated region at $\theta=90^o$ and r/r_{fan}=0.98 (Figure 10 a). This variation is significantly unsteady with a standard deviation of $\sigma=5.2^o$. As the ground clearance is increased to H/D_{hi}=0.44 and for the same crosswind velocity of V_{cw}=30kts (Figure 10 b), the separated region in the lower quadrant of the intake is associated with a similar mean value of Δi. For this configuration, the signal is also quite periodic, and the standard deviation is reduced with $\sigma=3.9^o$. For H/D_{hi}=0.44 and V_{cw}=36kts (Figure 10 c) the signal is notably unsteady. This is due to a transient movement of the separation in the tangential direction. As a result, the standard deviation is increased to $\sigma=10.2^o$. However, the mean value is comparable with the other two configurations (Figure 10 a-b).

The spectrum of Δi is mainly associated with three dominant frequency ranges (Figure 10 a-c). Two of these



a. V_{cw}=30kts, H/D_{hi}=0.25 b. V_{cw}=30kts, H/D_{hi}=0.44 c. V_{cw}=36kts, H/D_{hi}=0.44

Figure 10 Time variation of Δi for (a.) H/D_{hi}=0.25, V_{cw}=30kts, (b.) H/D_{hi}=0.44, V_{cw}=30kts, (c.) H/D_{hi}=0.44, V_{cw}=36kts.

are at approximately the blade passing frequency (f/f_{bp}=1.0) and its first harmonic (f/f_{bp}=2.0). The high frequency signatures are related to the fan blades shocks and the resulting pressure pulses [15]. The other dominant signature is at very low frequency ($0.01<f/f_{8p}<0.25$), and it is associated with the separation. The amplitudes and the peak frequencies of these low frequency signatures vary substantially depending on the configuration. For example, for H/D_{hi}=0.25 and V_{cw}=30kts (Figure 10 a) a broad band of frequencies with a modest amplitude occurs within $0.01<f/f_{8p}<0.25$. For H/D_{hi}=0.44 and V_{cw}=30kts (Figure 10 b), the amplitudes are notably reduced.

Overall, the two types of gross separations (windward and bottom) are characterised by similar mean effects on Δi for r/r_{fan}=0.98. However, the unsteady fluctuations of Δi for the separation on the windward side are less periodic and with greater amplitudes compared to the separation in the lower quadrant.

3.4. Peak swirl distortion events in the relative frame of reference

The blade incidence angle varies both over time and across different spatial locations. Therefore, it is necessary to analyse the full unsteady aspect. To accurately capture these variations, the peak fluctuations of Δi should be assessed in the blade rotating frame of reference. It is beneficial if the swirl distortion events are sufficiently distant in the azimuthal direction to allow the fan to recover [5]. The intensity and the exposure ϕ to peak swirl event can be assessed to evaluate the compatibility of an intake design and configuration with a fan. In this section the flow features that are responsible for the variation in Δi and the associated peak events are investigated. This is achieved by tracking the peak distortion events for all the blades (Figure 11 a-b, Figure 12 a-b, Figure 13 a-b) together with the relative Mach number M_{rel} and the radial location R_{norm} associated with the flow distortion (Eq. (8)).

$$R_{norm} = \frac{r - r_{hub}}{r_{fan} - r_{hub}} \quad (8)$$

For H/D_{hi}=0.25, V_{cw}=30kts (Figure 11 a-b), the peak events with the highest azimuthal exposure are the ones associated with the swirl variation at the hub (hub, α>0 and hub, α>0). However, the resulting peak intensity (Figure 11 a-b) is modest ($|\Delta i_{peak}|$~10º). Conversely, the peak distortion events with the highest positive intensity are mainly related to the separation and low V_{ax} on the windward side. At the tip (Figure 11 a-b), some peak events reach an intensity about 4.5 times greater than those at the hub (Δi_{peak}~45º) and an exposure up to ϕ=80º. Also, the ground vortex generates positive peak distortion events (Δi_{peak} between 0º and 15º). These are associated with M_{rel}>1.0 (Figure 11 b), and R_{norm}~0.85-0.9 (Figure 11 a). The peak events associated with the positive swirl at the hub-GV, and the high V_{ax} region have negative values of Δi (Figure 11 a-b, Figure 9 a). Although the peak intensity is modest ($0º<\Delta i_{peak}<10º$), the exposure extends from ϕ=0º up to 100º. While the high V_{ax} is related to M_{rel}>1.0 (Figure 11 b) and high values of R_{norm}~0.85-0.9 (Figure 11 a), the positive swirl at the hub-GV is associated with M_{rel}<1.0 (Figure 11 b) and R_{norm}~0.6-0.75 (Figure 11 a). The GV is also related to highly negative Δi peak events (Δi_{peak} between -20º and -10º) at the tip (R_{norm}=0.75-0.92, Figure 11 a) due to α<0º with an exposure within ϕ=15-30º. Overall, for H/D_{hi}=0.25, the peak events characterised by the highest intensity are the ones associated with the windward separation and low V_{ax}. However, the GV generates peak distortion events that are characterised by M_{rel}>>1.0 at the tip (Figure 11 b).

For the same V_{cw}=30kts, when the ground clearance is increased to H/D_{hi}=0.44 (Figure 12 a-b), there is an asymmetry for the positive and negative Δi peak events regions at the hub. While the region with Δi>0 (hub, α<0) has an exposure of ϕ=190-220º, for the one with Δi<0 (Hub, α>0), the exposure is ϕ=90-140º. The ground vortex strength has decreased, along with the associated peak intensity of the Δi>0 ($0º<\Delta i_{peak}<10º$ for GV, α<0) and Δi<0 ($-15º<\Delta i_{peak}<0º$ for GV, α>0) events. The

intensity and the exposure associated with the separation have also reduced, as the separation in the lower quadrant has a smaller azimuthal extent compared to the separation on the windward side for H/D_{hi}=0.25, V_{cw}=30kts (Figure 11 a). Overall, for H/D_{hi}=0.44 the effects of the separation in the lower quadrant results in lower intensity and exposure of the peak events compared with the windward separation of H/D_{hi}=0.25. At the tip, the intensity of the positive peak events and the M_{rel} associated with the GV is also reduced when H/D_{hi} is

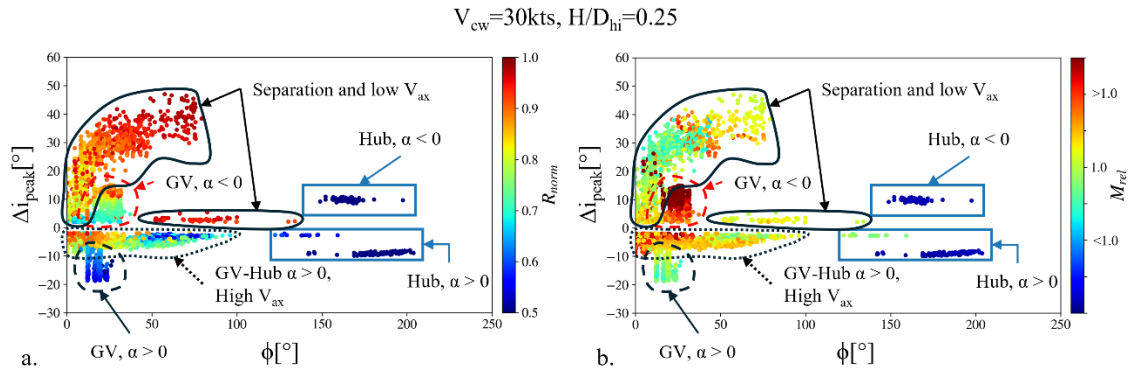


Figure 11 Peak swirl distortion events tracked for the fan blades for H/D_{hi}=0.25, V_{cw}=30kts, coloured by (a.) R_{norm} and (b.) $M_{rel.}$

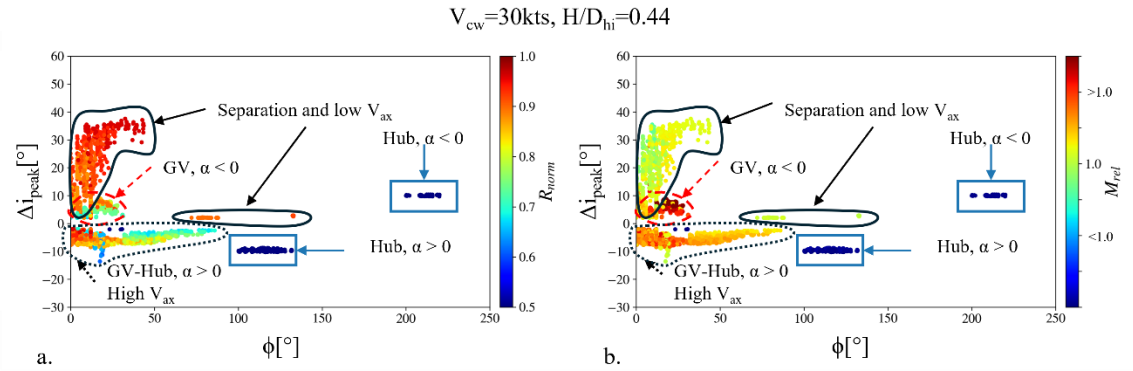


Figure 12 Peak swirl distortion events tracked for the fan blades for H/D_{hi}=0.44, V_{cw}=30kts, coloured by (a.) R_{norm} and (b.) $M_{rel.}$

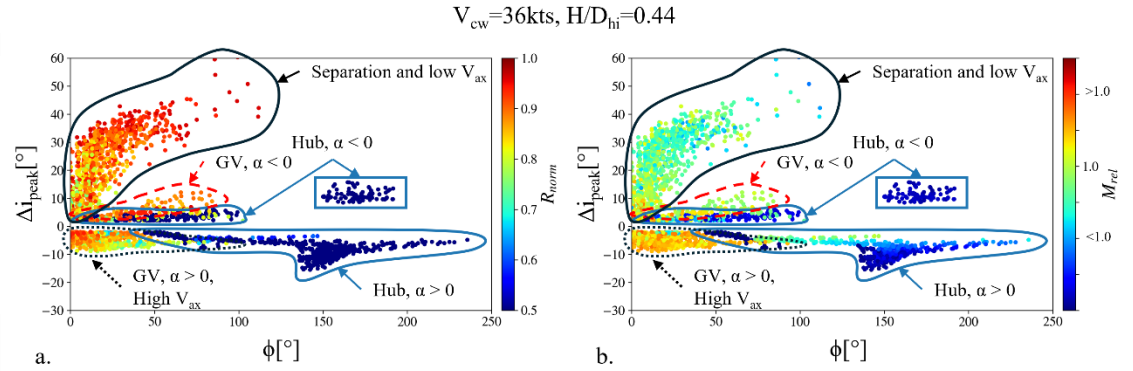


Figure 13 Peak swirl distortion events tracked for the fan blades for H/D_{hi}=0.44, V_{cw}=36kts, coloured by (a.) R_{norm} and (b.) $M_{rel.}$

increased.

For the large ground clearance H/D_{hi}=0.44 and V_{cw}=36kts (Figure 13 a-b), the intensity of the peak events related to the GV has further reduced as the GV has moved towards the intake surface ($0^o<|\Delta i_{peak}|<10^o$). However, the exposure has increased substantially up to exposure=90º. The peak events at the hub also have greater intensity ($|\Delta i_{peak}|$~10-15°) than for H/D_{hi}=0.44, V_{cw}=30kts (Figure 12 a-b) and H/D_{hi}=0.25, V_{cw}=30kts (Figure 11 a-b). Compared to V_{cw}=30kts, H/D_{hi}=0.44 (Figure 12 a-b), the maximum exposure of the peak events associated with $\alpha>0$ ($\Delta i>0$) at the hub has grown from ϕ=130º to 240º for H/D_{hi}=0.44 and V_{cw}=36kts (Figure 13 a-b). This increase in exposure can be either due to the transient phase (Section 3.3) or to a considerable change in the secondary flow patterns possibly due to the windward separation and the higher crosswind velocity (Figure 9 c). Compared to V_{cw}=30kts, H/D_{hi}=0.25 (Figure 11 a-b), the maximum exposure and peak intensity associated with the windward separation and low V_{ax} have increased up to Δi_{peak}=60° and ϕ=110° for H/D_{hi}=0.44 and V_{cw}=36kts (Figure 13 a-b). This variation can be due to a larger separation on the windward side, which originates at the lip due to the shock-boundary layer interaction.

Overall, significant differences in the unsteady intensity and exposure of the peak Δi events were identified. Both the exposure and the intensity are greater for the separation on the windward region (Figure 11 a-b, Figure 13 a-b) in comparison with the separation in the lower quadrant (Figure 13 a-b). Although the gross windward separation occurs at higher V_{cw} for H/D_{hi}=0.44 (Figure 13 a-b), the maximum intensity and exposure are greater compared to V_{cw}=30kts for H/D_{hi}=0.25 (Figure 11 a-b). While a larger ground clearance can be considered beneficial to improve the margin for the windward separation, once this occurs (V_{cw}=36kts), the associated swirl distortion could be greater (+15° for $\Delta i_{peak,}$ and +30° for ϕ) relative to H/D_{hi}=0.25, V_{cw}=30kts. These effects should be evaluated in the fan relative frame of reference when both the spatial and unsteady effects are taken into account.

4. Conclusions

A large variation of intake ground clearance was investigated for the first time with an unsteady fully coupled model of the intake/fan. The key contribution of this study is the identification of distinct characteristics of shock-driven separation due to significant changes in ground clearance. These findings challenge the common assumption that increased ground clearance is usually beneficial. It was demonstrated that gross separation can occur at lower crosswind velocities (-6kts compared with H/D_{hi}=0.25) and at the lower region of the intake rather than along the windward sideline. This behaviour is attributed to a mass flow redistribution, which directs more airflow toward the bottom lip. Conversely, the onset of the gross windward separation was improved for the larger ground clearance (+6kts with reference to H/D_{hi}=0.25) due to the off-loading of the sideline.

A further novelty of this study is in the assessment of unsteady swirl distortion and peak events in a relative frame of reference for a compact intake-fan system at full scale. The results indicate that for the larger ground clearance, the flow separation on the bottom-lip exhibits lower peak intensity and reduced exposure compared to windward separation across both H/D_{hi}=0.25 and 0.44 configurations. However, when windward separation occurs for the H/D_{hi}=0.44 configuration (V_{cw}=36kts), it leads to greater maximum intensity, exposure and temporal oscillations than the equivalent critical condition for H/D_{hi}=0.25 (V_{cw}=30kts).

Within an industrial context these findings highlight the necessity of evaluating intake designs at the expected ground clearance. Understanding the relationship between ground clearance, separation mechanisms, and swirl distortion is essential to optimise intake performance and ensure robust design choices under crosswind conditions.

5. Acknowledgements

L. Lobuono was supported by the Engineering and Physical Sciences Research Council [grant number EP/W524529/1], Rolls Royce plc., and Cranfield University. D. MacManus and R. Christie were partially funded by Innovate UK ATI FANFARE project (Ref: 113286).

6. REFERENCES

[1] A. Peters, Z. S. Spakovszky, W. K. Lord, and B. Rose, “Ultrashort nacelles for low fan pressure ratio propulsors,” *J Turbomach*, vol. 137, no. 2, Feb. 2015, doi: 10.1115/1.4028235.

[2] T. Cao, N. R. Vadlamani, P. G. Tucker, A. R. Smith, M. Slaby, and C. T. J. Sheaf, “Fan–intake interaction under high incidence,” *J Eng Gas Turbine Power*, vol. 139, no. 4, p. 041204, 2017, doi: 10.1115/1.4034701.

[3] T. Piovesan, P. K. Zachos, D. G. MacManus, and C. Sheaf, “Unsteady Swirl Distortion in a Short Intake Under Crosswind Conditions,” *AIAA Journal*, pp. 1–18, Dec. 2024, doi: 10.2514/1.J064226.

[4] W. Zhang and M. Vahdati, “A parametric study of the effects of inlet distortion on fan aerodynamic stability,” *J Turbomach*, vol. 141, no. 1, Jan. 2019, doi: 10.1115/1.4041376.

[5] A. Awes, A. Brosse, G. Dufour, X. Carbonneau, and B. Godard, “Effect of a vortex distortion on the operability of an ultra-high bypass ratio fan,” in *Proceedings of the ASME Turbo Expo 2020:*

Turbomachinery Technical Conference and Exposition. Volume 2A: Turbomachinery, 2020. doi: 10.1115/GT2020-14596.

[6] W. Zhang, "Influence of inlet distortion on fan aerodynamic performance," PhD thesis, Imperial College London, 2019.

[7] J. P. Murphy and D. G. MacManus, "Intake ground vortex prediction methods," *J Aircr*, vol. 48, no. 1, pp. 23–33, 2011, doi: 10.2514/1.46221.

[8] A. N. Rao, P. Sureshkumar, S. Stapelfeldt, B. Lad, K.-B. Lee, and R. P. Rico, "Unsteady Analysis of Aeroengine Intake Distortion Mechanisms: Vortex Dynamics in Crosswind Conditions," *J Eng Gas Turbine Power*, vol. 144, no. 12, Oct. 2022, doi: 10.1115/1.4055279.

[9] S. Zantopp, D. MacManus, and J. Murphy, "Computational and experimental study of intake ground vortices," *Aeronautical Journal*, vol. 114, no. 1162, pp. 769–784, 2010, doi: 10.1017/S0001924000004255.

[10] N. Mishra, D. MacManus, and J. Murphy, "Intake ground vortex characteristics," *Proc Inst Mech Eng G J Aerosp Eng*, vol. 226, no. 11, pp. 1387–1400, Nov. 2012, doi: 10.1177/0954410011424092.

[11] L. Boscagli, R. Christie, D. MacManus, and T. Piovesan, "Aerodynamics of a short intake in crosswind," *Aerosp Sci Technol*, vol. 129, p. 107826, Aug. 2022, doi: 10.1016/j.ast.2022.107826.

[12] L. Boscagli, D. MacManus, and R. Christie, "Fan-intake aerodynamic interactions under crosswind conditions," in *15th European Conference on Turbomachinery Fluid dynamics & Thermodynamics, 24-28 April 2023, Budapest, Hungary*, Jan. 2023. doi: 10.29008/ETC2023-303.

[13] A. C. Pardo, E. J. Gunn, T. S. Williams, C. A. H. Hall, T. Brandvik, and S. Baralon, "Crosswind aerodynamics of low pressure ratio fans," in *Proceedings of Global Power and Propulsion Society, GPPS Chania24*, Global Power and Propulsion Society, Sep. 2024. doi: 10.33737/gpps24-tc-097.

[14] D. A. Nichols, B. Vukasinovic, A. Glezer, and B. Rafferty, "Formation of a Nacelle Inlet Ground Vortex in Crosswind," in *AIAA SCITECH 2022 Forum*, American Institute of Aeronautics and Astronautics, 2022. doi: 10.2514/6.2022-1698.

[15] L. Lobuono, D. MacManus, R. Christie, and L. Boscagli, "Unsteady aerodynamics of a coupled compact intake-fan in crosswind," in *ICAS PROCEEDINGS 34th Congress of the International Council of the Aeronautical Sciences*, Florence: The International Council of the Aeronautical Sciences, Sep. 2024.

[16] R. Christie, A. Heidebrecht, and D. MacManus, "An automated approach to nacelle parameterization using intuitive class shape transformation curves," *J Eng Gas Turbine Power*, vol. 139, no. 6, p. 062601, 2017, doi: https://doi.org/10.1115/1.4035283.

[17] R. Christie, M. Robinson, F. Tejero, and D. G. MacManus, "The use of hybrid intuitive class shape transformation curves in aerodynamic design," *Aerosp Sci Technol*, vol. 95, p. 105473, 2019, doi: https://doi.org/10.1016/j.ast.2019.105473.

[18] K.-B. Lee, M. Wilson, and M. Vahdati, "Effects of Inlet Disturbances on Fan Stability," *J Eng Gas Turbine Power*, vol. 141, no. 051014, 2018, doi: 10.1115/1.4042204.

[19] P. Moinier, "Algorithm Developments for an Unstructured Viscous Flow Solver," PhD Thesis, University of Oxford, 1999.

[20] G. Almendral-Fernandez, D. Amirante, and N. J. Hills, "Use of a zonal hybrid URANS-LES methodology for prediction of rim seal ingestion into a low pressure turbine cavity," in *2018 Joint Propulsion Conference*, American Institute of Aeronautics and Astronautics Inc, AIAA, 2018. doi: 10.2514/6.2018-4917.

[21] L. Boscagli, D. MacManus, R. Christie, and C. Sheaf, "Effect of Unsteady Fan-Intake Interaction on Short Intake Design," *J Eng Gas Turbine Power*, vol. 146, no. 3, Nov. 2023, doi: 10.1115/1.4063768.

[22] T. Cao, N. R. Vadlamani, P. G. Tucker, A. R. Smith, M. Slaby, and C. T. J. Sheaf, "Fan-Intake interaction under high incidence," *J Eng Gas Turbine Power*, vol. 139, no. 4, 2017, doi: 10.1115/1.4034701.

[23] N. R. Vadlamani, T. Cao, R. Watson, and P. G. Tucker, "Toward future installations: Mutual interactions of short intakes with modern high bypass fans," *J Turbomach*, vol. 141, no. 8, Aug. 2019, doi: 10.1115/1.4044080.

[24] M. Carnevale, F. Wang, and L. Di Mare, "Low Frequency Distortion in Civil Aero-engine Intake," *J Eng Gas Turbine Power*, vol. 139, no. 4, Apr. 2017, doi: 10.1115/1.4034600.

[25] J. W. Cooley and J. W. Tukey, "An Algorithm for the Machine Calculation of Complex Fourier Series," 1964.

[26] M. Migliorini, P. K. Zachos, and D. G. Macmanus, "Novel Method for Evaluating Intake Unsteady Flow Distortion," *J Propuls Power*, vol. 38, no. 1, pp. 135–147, 2022, doi: 10.2514/1.B38127.



https://dspace.org/

Unsteady flow interactions and ground plane proximity in a coupled compact intake-fan in crosswind

Lobuono, Luca; MacManus, David G.; Hueso Rebassa, Josep; Christie, Robert

2025-04-01
Association Aeronautique et Astronautique de France (3AF)
https://doi.org/10.60711/aero2025.20250401.8402130248130544
Lobuono L, MacManus D, Hueso Rebassa J, Christie R. (2025) Unsteady flow interactions and ground plane proximity in a coupled compact intake-fan in crosswind. In: 59th 3AF International Conference on Applied Aerodynamics, 24 - 26 Mar 2025, Strasbourg, France

Downloaded from a DSpace repository. https://dspace.org/